Vol. 38, No. 1
March 2020

JOURNAL OF
RADIATION
EFFECTS
Research and Engineering

Analysis of an Energy Tuning Assembly for Simulating Nuclear Weapon Environments at the National Ignition Facility

N.J. Quartemont, J.E. Bevins, R.N. Slaybaugh, and L.A. Bernstein

This paper was presented at the 36th Annual HEART Conference, San Diego, CA, April 8–12, 2019. It received the Best Student Paper Award.

Prepared by Amentum for the HEART Society under contract to NSWC Crane

This material is based upon work supported in part by the National Science Foundation Graduate Research Fellowship under grant no. NSF 11-582. This work is also supported by the U.S. Air Force Technical Application Center (AFTAC) under the AFIT/AFTAC Endowed Term Chair MOA#: 212196 and the Defense Threat Reduction Agency under grant HDTRA-18-27434. The views expressed in this paper are those of the authors and do not necessarily reflect the official policy or position of the United States Air Force, the Department of Defense, or the United States Government.

ANALYSIS OF AN ENERGY TUNING ASSEMBLY FOR SIMULATING NUCLEAR WEAPON ENVIRONMENTS AT THE NATIONAL IGNITION FACILITY

N.J. Quartemont and J.E. Bevins
Air Force Institute of Technology, Department of Engineering Physics
Wright-Patterson Air Force Base, OH

R.N. Slaybaugh and L.A. Bernstein
University of California, Berkeley, Nuclear Engineering Department
Berkeley, CA

Abstract

An energy tuning assembly (ETA) was developed to spectrally shape the National Ignition Facility (NIF) deuterium-tritium (D-T) fusion neutron source to a notional thermonuclear and prompt fission neutron spectrum (TN+PFNS) to approximate a boosted nuclear device. The spectrally shaped neutron environment can be used to create realistic synthetic post-detonation weapon debris that contain spectrally accurate fission products across all mass chains to enhance U.S. technical nuclear forensics capabilities for nuclear weapon attribution and device reconstruction. This research performed nuclear data covariance analysis through stochastic sampling techniques to predict the performance of an ETA to create the objective TN+PFNS, assess anticipated experimental outcomes, and determine the expected fission products to be produced in a highly enriched uranium foil in the sample cavity. It was found that the nuclear data covariance affected the neutron fluence energy distribution by less than 5 percent for neutron energies above 1 keV in the sample region. The foil activation resulting from the perturbed fluence distribution was found to generally vary on the order of 3–5% but was as high as 20%. The range of foil activation outcomes was used to show that neutron-flux unfolding techniques provided broad spectral agreement between the ETA and objective spectrum and resulted in an 80+% probability of successful unfolding using STAYSL given the range of expected foil activities. This energy distribution was achieved at a total fluence of 4.9 x 10^{11} n cm^{-2} ±1.4% in a 10-shake neutron pulse. More than 1 billion fissions, approximately of the order collected in nuclear forensics ground samples, were generated with a cumulative fission product distribution that matched the objective within current predictive capabilities. The analysis performed in this research enables the development of a NIF validation experiment, enhances confidence in the experimental outcomes, and further develops a unique capability for the nuclear security community.

Introduction

Generating neutron environments has broad application to the nuclear forensics, medical, national security, and nuclear data communities [1]–[3]. The neutron energy spectrum is important for many applications, such as the survivability of electronics in strategic environments, and deviations from the threat environment for testing have many implications for the certification of nuclear components [4]. Additionally, accurate neutron energy distributions are critical to the production of accurate fission product samples that have a direct impact on the deterrence of potential nuclear terrorism through the development and improvement of nuclear attribution capabilities [5]. However, no capability exists to replicate nuclear weapon neutron environments in the absence of full-scale testing [6]. Alternative methods of creating fission product debris have been explored to include sample doping, direct production using fission converters, or surrogate methods [7]. Each of these methods are limited in their ability to correctly reproduce the expected fission product distribution resulting from the neutron environment experienced in a nuclear weapon.

This material is based upon work supported in part by the National Science Foundation Graduate Research Fellowship under grant no. NSF 11-582. This work is also supported by the U.S. Air Force Technical Application Center (AFTAC) under the AFIT/AFTAC Endowed Term Chair MOA#: 212196 and the Defense Threat Reduction Agency under grant HDTRA-18-27434. The views expressed in this paper are those of the authors and do not necessarily reflect the official policy or position of the United States Air Force, the Department of Defense, or the United States Government.

JOURNAL OF RADIATION EFFECTS,
Research and Engineering
Vol. 38, No. 1, March 2020

An alternative approach is to develop a neutron energy spectrum representative of an objective neutron energy spectrum. This can be accomplished through targeted modification of a source neutron energy distribution, a non-trivial process for neutrons. To automate the process for designing energy tuning assemblies (ETAs), the Coeus metaheuristic optimization software package was developed to convert a facility's characteristic source spectrum to a user-defined objective spectrum [8], [9]. Coeus enables fast and accurate design of ETAs to spectrally shape a given neutron spectrum into a desired neutron environment. As an example, the production of a nuclear weapon neutron spectrum was chosen to be used for the production of realistic fission debris. Coeus was used to develop an ETA with the objective of creating a surrogate nuclear weapon spectrum to produce accurate fission products to advance the technical nuclear forsenics field. The ETA is planned for a proof-of-concept experiment at the National Ignition Facility (NIF).

Initial validation of the spectral shaping and ETA concept was performed at the 88-Inch Cyclotron at Lawrence Berkeley National Laboratory. While this experiment demonstrated the concept, the 88-Inch Cyclotron source spectrum differed significantly from the NIF. This differing energy range covered nuclear data and reactions not applicable with the NIF deuterium-tritium (D-T) source and changed the relative weighting of the reaction channels important to the resulting neutron spectrum [10]. This is important because the spectral shaping concept breaks from traditional integral nuclear validation efforts in that the measurable outcomes are heavily dominated by specific reaction channels that vary based on material position in the ETA [11]. As such, while the 88-Inch provided the first validation of the concept, it provided little direct evidence of the performance of the ETA at the NIF. This is further compounded by the use of nontraditional nuclear materials in the ETA design, where the nuclear data quality may be poor. Therefore, this work sought to characterize the nuclear data uncertainty and its effect on the experimental observables of the ETA to better assess the performance of the system.

Unfortunately, quantifying the impact of nuclear data on complex systems with multiple observable signatures of interest is a non-trivial problem. Variance in the nuclear data affects the neutron transport simulation and the resulting modified neutron spectrum obtained after the source spectrum is modified through nuclear reactions. The resulting variance in the obtained neutron spectrum is then propagated to the observable reaction rates in the sample region inside of the ETA. This analysis incorporated nuclear data covariance into the simulated results through stochastic sampling of the underlying nuclear data to build a distribution of responses [12]. The cross section libraries used in this work were Evaluated Nuclear Data File/B-Version (ENDF/B)-VII.1 for the neutron transport and the International Reactor Dosimetry and Fusion File (IRDFF) v.1.05 library for foil activation cross sections [13], [14].

Previous work completed the design of an ETA for the production of spectrally accurate fission product generation, initial experimental validation, and techniques to quantify the effect of nuclear data covariance [10], [12], [15]. The objective of this work is to model the ETA capability to tailor the NIF neutron energy spectrum and generate fission products for technical nuclear forensics applications, including reporting progress since previous work. This paper is organized as follows. First, the problem description of the ETA and design are provided. The next section provides the methodology for the main components of this research, including the Monte Carlo simulation, neutron fluence unfolding, and fission product estimation. Next, the results of the neutron transport calculation, unfolded spectrum, and fission product distributions are provided. Finally, the last section summarizes the major findings and provides a path forward for future work.

Model Description

The objective spectrum chosen for the production of synthetic weapon fission product debris was a thermonuclear and prompt fission neutron spectrum (TN+PFNS), which is representative of a boosted nuclear weapon neutron environment relevant to production of synthetic-fission product debris. The representative neutron spectrum was produced with Monte Carlo N-Particle (MCNP) Code 6.1 using transport in a bare Godiva sphere of a Watt fission spectrum and a 14.1-MeV source to model the D-T fusion neutrons [7], [16]. For the purposes of this study, several fission isotope yields of interest were se-

lected from the wings, valley, and peaks of fission product distribution for ^{235}U. Each fission product has energy-dependent data in the literature [13], [17]–[25].

The source selected was an NIF D-T polar-drive exploding-pusher (PDXP) target with a nominal yield of 3.7 x 10^{15} neutrons from laser-driven, inertial-confinement fusion [26]. The D-T fusion produces 14-MeV energy neutrons that fill in the thermonuclear component of the objective spectrum, and the prompt fission portion is built up with neutron interactions in the ETA. The prompt nature of the irradiation negates decay and ingrowth errors associated with long irradiation times.

The ETA produced with Coeus to meet the objective notional TN+PNFS is shown in Fig. 1 [7]. The NIF source was located 15 cm below the base of the cone. The ETA was constructed with cones and cylinders using materials of boron carbide, praseodymium, stainless steel, bismuth, tungsten, silicon, and lead. The external portions of ETA and surroundings were filled with vacuum pressure nitrogen below 10^{-4} torr [27]. The ETA sample cavity (labeled 6 in Fig. 1) was encased in a lead-filled, removable drawer (labeled 8 in Fig. 1) for rapid sample extraction post-irradiation. The ETA was modeled with the drawer facing up, so that the direction of gravity skewed the mass distribution away from the drawer insert. The model is available on a GitHub repository [28].

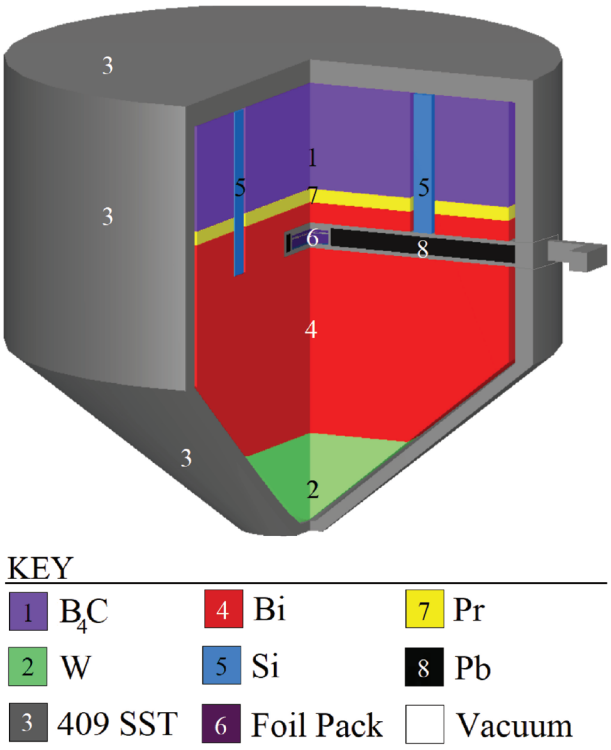

Figure 1. ETA produced by Coeus to reproduce an objective notional TN+PFNS [7].

The ETA sample cavity is designed to hold several activation foils and a highly enriched uranium (HEU) sample in a target option activation device (TOAD). The foils chosen were natural indium (In), aluminum (Al), nickel (Ni), zirconium (Zr), gold (Au), tungsten (W), and manganese (Mn). These foils have threshold and non-threshold reactions that span the range of interest from the TN+PFNS energy spectrum, which can be used to unfold the incident neutron energy spectrum to validate the ETA performance [29], [30]. The HEU sample is enriched to 93.15% and is the source of the fission products.

A summary of the foil characteristics for the reactions chosen for the simulated NIF experiment is shown in Table 1. The Zr, Ni, In, Al, W, and Mn foils were all 1 mm in thickness and 2.5 cm in radius. The foils were selected to cover threshold energy reaction channels and thermal reactions that inform lower-energy neutron-flux environments. The Au foil was 0.0254-mm thick with a radius of 2.004 cm. The HEU foil not shown in the table was 2.004 cm in radius and 0.0508 mm in thickness.

Description of Work

This section describes the overarching methodology for the radiation transport simulation and the quantification

Table 1. Selected activation foil information for simulated NIF experiment.

Reaction	Threshold [MeV] (@ 10 mb)	Decay Radiation [keV] (Intensity)
^{90}Zr (n,2n)	12.1 (12.1)	909.2 (0.9904)
^{58}Ni (n,2n)	12.4 (13.3)	1,378 (0.817)
^{58}Ni (n,p)	0.4 (1.3)	810.8 (0.9945)
^{197}Au (n,2n)	8.1 (8.3)	355.7 (0.87)
^{197}Au (n,g)	Thermal	411.8 (0.9562)
^{115}In (n,n')	0.336 (0.597)	336.24 (0.459)
^{115}In (n,g)	Thermal	1293.56 (0.848)
^{27}Al (n,a)	3.25 (6.7)	1368.63 (0.9999)
^{186}W (n,g)	Thermal	685.51 (0.332)
^{55}Mn (n,g)	Thermal	846.8 (0.9885)

JOURNAL OF RADIATION EFFECTS,
Research and Engineering
Vol. 38, No. 1, March 2020

of nuclear data uncertainty. Additionally, the technique used to unfold the neutron fluence from the modeled activation foil activities is presented. Finally, two methods for predicting fission products are outlined.

Neutron Transport Simulations

The simulation methodology to propagate nuclear data covariance through the ETA design included neutron transport calculations in MCNP5 and the Standardized Computer Analysis for Licensing Evaluation (SCALE) code package [31], [32]. Additional systematic uncertainties due to materials and geometry were limited through the use of 99.5+% pure components and sub-mm machining tolerances on each component in the constructed ETA. MCNP5 was used for continuous-energy Monte Carlo neutron transport, which was used to benchmark continuous-energy Monte Carlo neutron transport in SCALE Monaco with Automated Variance Reduction using Importance Calculations (MAVRIC). The SCALE MAVRIC sequence was utilized for Monte Carlo radiation transport in continuous energy to validate the model to MCNP and was also used in a 252 energy group structure with the SCALE Sampler module to assess the effect of nuclear data covariance [32]. Finally, the activation foil uncertainties were sampled with a multivariate normal distribution to incorporate the reaction cross-sectional uncertainty consistent with the IRDFF v.1.05 nuclear data library [12], [14].

The SCALE Sampler module enabled analysis of nuclear data covariance through pre-built libraries based on stochastic sampling of the nuclear data and was distributed with a 252 and 56 energy group structure [32]. The covariance libraries were largely developed from ENDF/B-VII.1; however, additional information was included from collaborative research between Brookhaven National Laboratory, Los Alamos National Laboratory, and Oak Ridge National Laboratory. Additionally, the nuclear data covariance libraries included information completed in the Working Party on International Nuclear Data Evaluation Cooperation Subgroup-26 [32]. The impact of nuclear data covariance was addressed for the neutron energy spectrum, foil activation rates, and fission product production rates. The output from Sampler was used with the IRDFF covariance matrices to generate final response metrics with systematic uncertainty from the radiation transport and reaction cross sections [12]. The IRDFF library contains benchmarked neutron dosimetry reactions and "state-of-the-art" covariance information [33].

A validated, full-scale NIF model did not exist for the SCALE package, but significant development and validation of the full NIF model has been performed in MCNP5 [31]. As such, the ETA was modeled in MCNP5 with a surface source read (SSR) file generated using a 14.03-MeV neutron point source, which is the zero ion-temperature mean energy [34]. NIF neutron emissions are extremely short in duration, on the order of 300 picoseconds, so the neutrons were modeled as all being generated at the same time [26]. The SSR source included a full system model of NIF that included the target positioner, ETA, ETA diagnostic instrument manipulator (DIM), snout DIM, and target chamber support structures. The SSR file reads in a formatted file that contains all of the particle histories that cross defined surfaces, thereby allowing for accelerated transport in regions of interest [31], [35]. This allowed the Sampler models to capture the impact of room return without requiring the creation of a full NIF model in SCALE.

The SSR file surfaces used were two disks at the front and back of the ETA and a connecting cylinder surrounding the ETA. The SSR generated in MCNP was mapped to probability distribution functions with relative strengths for each primary surface. The surface neutron current distributions at the front (source facing), back, and cylindrical surfaces are shown in Fig. 2. The back and cylindrical surfaces solely represented the room return, while

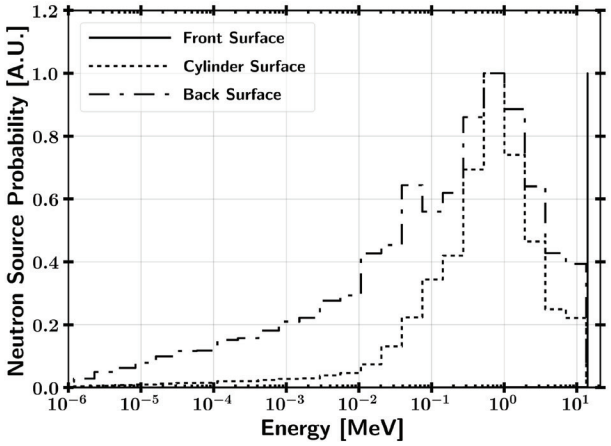

Figure 2. Surfaces source probability distribution functions generated from the MCNP SSR for use in SCALE. The distributions were normalized to a peak value of 1.

the front source was dominated by source neutrons. The total fluence of neutrons through the front, back, and cylindrical surfaces were 6.5×10^{14}, 3.5×10^{12}, and 2.4×10^{12} neutrons, respectively.

The neutron current on the SSR surfaces in MCNP5 was mapped to SCALE for use in MAVRIC and Sampler by source definitions to approximate the behavior of MCNP's surface source. The front source was modeled as a point source at the location of the PDXP target. The point-source strength was 3.72×10^{15} neutrons, which included the room return component, based on the solid angle between the front surface and the point source. Cylindrical neutron sources could not be adapted to Cartesian coordinate direction vectors, so the cylindrical SSR surface was approximated. The back source was modeled as a disk, and the cylinder was approximated as four line sources placed symmetrically at the same distance from the ETA as the original SSR cylindrical source facing the ETA and emitting in 2π.

The MCNP5 model was compared to the continuous energy MAVRIC sequence to benchmark the sources used for MAVRIC and the 252-group Sampler values. The resultant model for the continuous energy SCALE MAVRIC sequence was converted to the 252-group SCALE Sampler sequence, where the nuclear data covariance was assessed. The 252-group structure was built for nuclear reactor applications, which is non-ideal for this application and resulted in some discrepancies near bin boundaries [12]. However, the 252 group was the best nuclear data covariance library available for SCALE Sampler at the time of this research. The Sampler values were collapsed at lower energy to create a 66-group structure.

The results of each of the models were used to assess the foil reactions and HEU fissions achieved in the ETA platform. Since the total neutron fluence time is much less than the half-lives of the fission and activation products for the foils, this removes any uncertainty from ingrowth and decay during the experiment. The resultant responses were combined using statistical bootstrapping, where confidence bounds were determined by randomly selecting with replacement data from the sampled distributions to create a probability distribution representative of the underlying distribution [36].

Sampler was used to generate 182 trials to provide converged results for all of the activation foil reactions, HEU fissions, and neutron fluence, including the post-processing perturbations with the IRDFF nuclear data covariance. The convergence of ^{56}Mn production, which contained the largest uncertainty and was least converged—thereby representing the worst-case performance—is shown in Fig. 3. In all cases, the bootstrapped mean value was within 1% of the unperturbed nuclear data starting sample. The response values from Sampler and MCNP5 for the activation foil reactions, neutron fluence, and HEU fissions were determined with the continuous energy values from MCNP5 and the uncertainty bounds given by the quadrature addition of the MCNP5 statistical error and Sampler systematic error attributed to nuclear data covariance.

Finally, the reaction results from Sampler were again sampled with a multivariate normal distribution to perturb the data consistent with the IRDFF v.1.05 library [12]. The user-defined responses used in Sampler were not modified in the Monte Carlo simulations, so the uncertainty in the foil reaction cross sections needed to be taken into account in post-processing due to limitations in SCALE. ENDF data was utilized for ^{55}Mn (n,g), ^{186}W (n,g), and U (n,f) because it was consistent with IRDFF [13], [14]. The reaction cross section was modified in the execution of Sampler for these three reactions sets and required no subsequent post-processing [13].

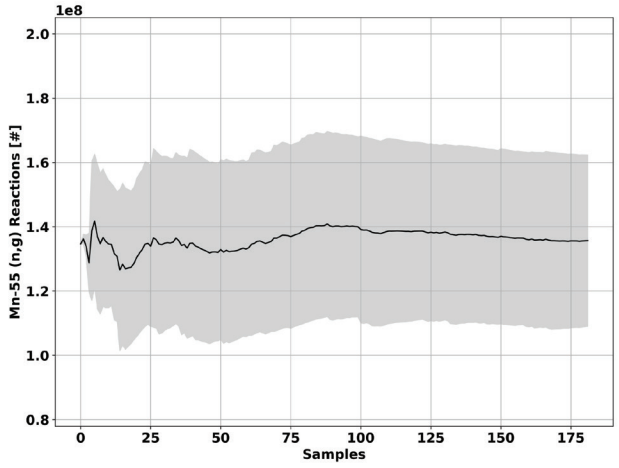

Figure 3. Cumulative moving average ^{56}Mn production vs. sample number with starting value shown as the black solid horizontal line.

JOURNAL OF RADIATION EFFECTS,
Research and Engineering
Vol. 38, No. 1, March 2020

Neutron Spectra Statistical Tests

The results of the Monte Carlo simulations were compared to the TN+PFNS through the Pearson correlation coefficient and the Kolmogorov-Smirnov (K-S) statistic. The Pearson correlation coefficient provides a measure of the linear relationship between two sets of data and is often used for comparative signal analysis. The formula for the Pearson correlation coefficient is given as a function of "n" data points for two distributions defined by points x_i and y_i as

$$r = \frac{n\sum x_i y_i - (\sum x_i \sum y_i)}{\sqrt{n\sum x_i^2 - (\sum x_i)^2}\sqrt{n\sum y_i^2 - (\sum y_i)^2}}. \quad (1)$$

The null hypothesis of the Pearson correlation coefficient is that there is no correlation between the two data sets. The p-value indicates the probability of an uncorrelated system producing a correlation coefficient at least as large in magnitude. Small p-values (<0.05) indicate a statistically significant Pearson correlation coefficient.

The K-S two-sample statistic compares the cumulative distribution functions (CDFs) between two sets of data. The K-S statistic provides information on the relative magnitude of the distributions, so it is useful in combination with the Pearson correlation coefficient to quantify the similarity between two distributions. The K-S statistic is given as a function of the supremum (maximum) difference between the expected and observed CDF as shown in (2). The null hypothesis for this test is that the two samples were drawn from the same distribution. Unlike the Pearson correlation coefficient, a large p-value (>0.05) from the K-S statistic fails to reject the null hypothesis.

$$D = \sup_x | CDF_{exp}(x) - CDF_{obs}(x) | \quad (2)$$

Neutron Fluence Unfolding

The modeled foil activities were used with the underlying IRDFF nuclear data to unfold the neutron spectrum using STAYSL [37]. STAYSL determines the incident neutron flux using a generalized least-squares spectral adjustment based on a χ^2 comparison of the measured activities and the activities calculated from an adjusted flux [33]. STAYSL utilizes activity information (A°), a neutron flux, a nuclear data matrix (P), and covariance matrices in the formulation of the χ^2 statistic. The χ^2 is minimized based on the STAYSL minimized activity information ($\bar{A}$) and the STAYSL calculated neutron flux convolved with the IRDFF nuclear data parameters ($\bar{P}$). The χ^2 statistic utilized in STAYSL is given by [38]

$$\chi^2 = \begin{bmatrix} P - \bar{P} \\ A^\circ - \bar{A} \end{bmatrix}^\dagger \bullet \begin{bmatrix} N_P & 0 \\ 0 & N_{A^\circ} \end{bmatrix}^{-1} \bullet \begin{bmatrix} P - \bar{P} \\ A^\circ - \bar{A} \end{bmatrix} \quad (3)$$

where N_P is the covariance matrix from the flux and nuclear data and N_{A° is the activity covariance matrix. For this work, the 129-group IRDFF v.1.05 library was used, which is ideal for dosimetry applications for the range of energies considered in this work [14].

The activities produced for a given set of foils are often degenerate, where an infinite number of spectra could provide the same distribution of measured activities. To overcome this, STAYSL requires an initial guess neutron spectrum to introduce a Bayesian prior, allowing for physics and modeling to guide the overall solution space. The initial guess spectrum used for STAYSL was the nominal MCNP-calculated neutron fluence in the HEU foil, and the specified uncertainty includes both the statistical and systematic nuclear data uncertainty.

The reduced chi-squared statistic (χ^2) was used to interpret the unfolded neutron flux agreement with the set of results from Sampler. The reduced χ^2, as used in the foil activation neutron flux unfolding, is [39]

$$\frac{\chi^2}{\nu} = \frac{1}{\nu}\sum_{i=1}^{N}\left(\frac{R_{Trial} - R_{STAYSL}}{\sigma_{rxn}}\right)^2 \quad (4)$$

where the degrees of freedom (ν) are the number of activation foil reactions (N) minus one, σ_{rxn} is the modeled systematic and statistical uncertainty, R_{STAYSL} is the unfolded STAYSL activation foil activity, and R_{Trial} is the Sampler trial foil activity.

The null hypothesis for the χ^2 statistic is that the two sets of data are governed by the expected distribution, and the test of independence shows the probability of rejecting this null hypothesis. The p-value, the probability of finding a larger χ^2/ν given the calculated result, can be used to compare the results of the expected distribution to the calculated χ^2/ν. A small p-value (<0.05) signifies there is a strong significance level for the results not

being governed by the expected distribution. P-values above the cutoff significance level fail to reject the null hypothesis.

Fission Product Estimation

The energy spectrum of neutrons causing fission was used to determine the fission product yield with a phenomenological fit and the General Description of Fission Observables (GEF) code [40]. The distribution of neutrons causing fission is proportional to the fission cross section times the neutron flux. Including fits to experimental data enables better energy resolution and predictions that are consistent with observed experiments where experimental data exists, while GEF enables predictions for mass chains lacking sufficient energy-dependent data. Empirical relations developed by Nagy *et al.* provide an approach to predict the fission product yield as a function of energy given sufficient yield measurement data [17]. Nagy fits the fission product experimental data to the exponential equation

$$Y(E_n) = Y_0 e^{bE_n} \tag{5}$$

where the fitting parameters b and Y_0 represent the slope of the function in logarithmic form and thermal fission yield, respectively [17]. The slope is the primary measure of the energy dependence of the fission product yield, which requires modifications for multi-chance fission. Modifications were performed to incorporate first- and second-chance fission, which are the most dominant modes up to 14.1 MeV. First-chance fission is dominant from up to 5.5 MeV, and second-chance fission up to 14.1 MeV [17]. Multi-chance fission effects on the fission product yield are less pronounced in asymmetric regions but can have a large impact in symmetric fission ($109 \leq A \leq 129$) [7], [17].

GEF is applicable over a wide range of fissioning systems, including isotopes with atomic numbers from 80 to 112 [40]. The underlying model has been shown to have good predictive power, albeit with relatively large uncertainties due to GEF containing up to 50 free parameters used for the potential energy surfaces of the fission barrier of the fissioning system, fission theory, and adjustments based on empirical parameters [41], [42]. GEF incorporates covariance information of the fissioning system, multi-chance fission, and many other unique features.

The values for the mass-chain yield distribution calculated by GEF were determined using separate calculations for each energy group defined by the midpoint bin energy of the fissioning system, ^{236}U for neutron-induced ^{235}U fission. The uncertainty reported includes a combination of the GEF Monte Carlo statistical and systematic uncertainty and the systematic uncertainty from the Sampler results for the fissioning neutron energy distribution.

Results

Using the methodology outlined above, the ETA was simulated to determine the nuclear impact of nuclear data on the overall performance and experimental observables. First, the results of the neutron transport are presented including the overall ETA fluence distribution, the foil activation, and the timing profile. Next, the results of the modeled neutron flux unfoldings are provided for each of the trials completed in Sampler. Last, the predicted fission product distribution for selected cumulative-yield fission products and the mass-chain fission product yield for the ETA neutron-spectrum-produced fissions are presented.

Neutron Transport Results

A summary of the activation foil reactions and fissions in the HEU foil are given in Table 2. A bias of approximately 1% was observed for the reaction rates from the continuous energy MAVRIC simulation, a result consistent with previous code comparison results [42]–[44]. However, there were some important discrepancies that are caused by the 252-group structure. The 252-group Sampler mean total reactions were generally in agreement with the continuous energy solutions with three exceptions: ^{89}Zr, ^{57}Ni, and ^{56}Mn. The first two threshold reactions were attributed directly to the flux weighting of the 13.8- to 14.6-MeV group used in the energy region where the reaction occurred. The 252-group ^{55}Mn reaction difference from MCNP was caused by the flux weighting used to create the group cross section, and the bulk of the difference occurred below 80 keV. The 252-group library performed well for the majority of the reactions because many of the activation reactions were saturated by the PFNS, which was used to generate the cross-sectional weighting for the intended nuclear reactor applications of this group structure.

The continuous energy solutions in Table 2, MCNP SSR and SCALE MAVRIC CE, only capture statistical uncertainty in their results. The 252-group SCALE Sampler results capture statistical and bootstrapped systematic nuclear data uncertainty from the Sampler results. As can be seen, the systematic nuclear data uncertainty greatly exceeds the contribution of the statistical uncertainty to the overall uncertainty of the simulated results. Inclusion of nuclear data uncertainty results in relative errors less than 5% for most reactions; however, ^{56}Mn production has a relative error of 19.7%.

The neutron-fluence results of the continuous energy MCNP5 and SCALE MAVRIC sequence in comparison to the notional objective TN+PFNS are shown in Fig. 4. Overall, there is broad neutron spectral agreement between the TN+PFNS and ETA fluence and between MCNP5 and SCALE. Comparing the nominal values, there are a few main areas of disagreement between the ETA result and TN+PFNS. First, below 50 keV, there is an increase in thermal neutrons in the ETA simulations relative to the objective spectrum; however, this portion of the spectrum only represents ~1% of the ETA fluence. The NIF room return and low-A spectral shaping components, necessitated by NIF weight constraints used in the design, contribute to the majority of this fluence. Additionally, from 7 to 14 MeV there are relatively large differences caused by the method used to generate the TN+PFNS. Godiva, composed solely of HEU, has very few pathways to populate this energy region. The primary energy-loss mechanisms in Godiva, inelastic scattering, and (n,xn) reactions are limited in their ability to populate the 7- to 14-MeV energy range, and there would need to be many elastic scattering events to populate this energy range from the 14-MeV fusion source given the high-A of the Godica assembly. The 14-MeV region disagreement is caused by the lack of attenuation of the source neutrons; the weight constraints of the ETA design for the NIF facility meant that additional attenuating material could not be added. Further, above 14 MeV there is a severely depressed neutron

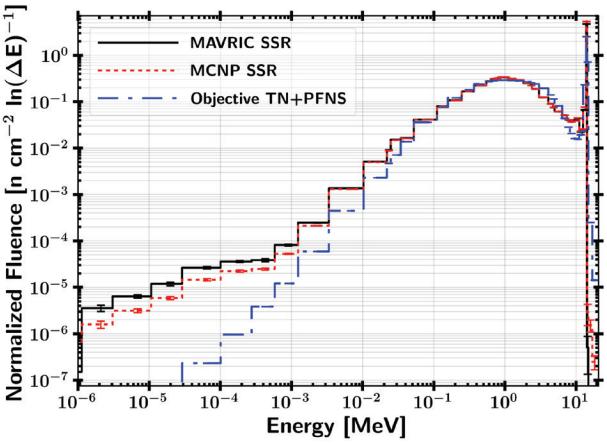

Figure 4. Normalized continuous energy MCNP5 SSR and SCALE-mapped SSR fluence per unit lethargy spectra comparison to objective TN+PFNS.

Table 2. Activation foil reaction results and HEU fissions modeled results from MCNP5, SCALE MAVRIC, and SCALE Sampler.

	MCNP SSR	SCALE MAVRIC CE		SCALE Sampler 252-Group	
Reaction	Reactions [#]	Reactions [#]	Percent Change Relative to MCNP	Reactions [#]	Percent Change Relative to MCNP
^{90}Zr (n,2n) ^{89}Zr	1.89E+9 ± 2.5E+6	1.91E+9 ± 1.4E+6	1.5	2.06E+9 ± 9.6E+7	9.0
^{58}Ni (n,2n) ^{57}Ni	1.87E+8 ± 2.4E+5	1.90E+8 ± 1.4E+5	1.4	2.21E+8 ± 1.1E+7	17.8
^{58}Ni (n,p) ^{58}Co	6.54E+9 ± 5.2E+6	6.64E+9 ± 1.5E+5	1.5	6.66E+9 ± 1.7E+8	1.7
^{197}Au (n,2n) ^{196}Au	2.91E+9 ± 3.8E+6	2.91E+9 ± 2.5E+6	-0.1	2.94E+9 ± 1.4E+8	1.0
^{197}Au (n,g) ^{198}Au	1.00E+9 ± 8.0E+5	1.02E+9 ± 1.5E+6	2.0	9.88E+8 ± 2.5E+7	-1.2
^{115}In (n,n') ^{115}In^{m1}	3.81E+9 ± 1.9E+6	3.82E+9 ± 1.7E+6	0.0	3.85E+9 ± 9.0E+7	1.0
^{115}In (n,g) ^{116}In^{m1}	5.14E+9 ± 2.6E+6	5.19E+9 ± 4.4E+6	1.0	5.12E+9 ± 1.8E+8	-0.3
^{27}Al (n,a) ^{24}Na	1.08E+9 ± 1.3E+6	1.08E+9 ± 7.7E+5	0.0	1.07E+9 ± 4.9E+7	-0.9
^{186}W (n,g) ^{187}W	7.21E+8 ± 7.2E+5	7.30E+8 ± 1.6E+6	1.2	7.08E+8 ± 2.9E+7	-1.9
^{55}Mn (n,g) ^{56}Mn	3.14E+8 ± 3.1E+5	3.23E+8 ± 4.7E+5	2.8	2.67E+8 ± 5.3E+7	-14.9
^{235}U(n,f)	1.94E+9 ± 1.2E+6	1.96E+9 ± 8.2E+5	0.5	1.95E+9 ± 2.1E+7	0.0
^{238}U(n,f)	2.70E+7 ± 2.4E+4	2.67E+7 ± 1.6E+4	-1.1	2.70E+7 ± 4.6E+5	0.0
Total Fissions	1.99E+9 ± 1.2E+6	2.00E+9 ± 8.4E+5	0.5	1.99E+9 ± 2.1E+7	0.0

flux in the ETA. A portion of this disagreement was caused by the mono-energetic source implementation instead of a more realistic ion-temperature-broadened distribution, which was chosen for consistency with previous NIF MCNP modeling work [34].

The results of the nuclear data covariance fluence spectra are shown in Fig. 5. The SCALE results were calculated with the 252-group structure and 182 samples from Sampler, while the MCNP5 results were performed with a continuous energy calculation using mapped, systematic nuclear data uncertainties from Sampler. The nuclear data covariance increases the flux uncertainty more significantly at lower energies where the transport is dominated by a cascade of multiple reactions. In general, the mean of the flux accounting for nuclear data covariance with Sampler is comparable to flux with the nominal nuclear data. Most of the difference in the mean value is due to differences in the underlying codes, as shown in Fig. 4, not due to a shift induced by the distribution of the nuclear data covariance captured in the Sampler results. Including the nuclear data covariance increases the range of potential values, approximately 3–5% above 1 keV and 7–100% below 1 keV.

The Pearson correlation coefficient and K-S two-sample statistic were used to test the statistical significance of the correlation between the ETA-generated spectrum and the objective TN+PFNS. Comparing the objective TN+PFNS to the continuous energy MCNP results yields a Pearson correlation coefficient of 0.90 ($p \ll 0.05$) and K-S statistic of 0.11 (p=0.11). The Pearson correlation coefficient result indicates that no correlation between the data sets can be rejected with strong significance, and the K-S statistic indicates the null hypothesis that samples drawn from the same distribution could not be rejected. The results indicate that Coeus-generated ETAs are able to succeed in closely replicating the TN+PFNS neutron environment based on the simulated results.

The incident fluence on the HEU foil for the modeled ETA experiment is 4.9 x 10^{11} n cm^{-2} ± 1.4%. The neutron fluence per unit area from an unshaped point source with a strength of 3.7 x 10^{15} neutrons at 29 centimeters (distance from the source to the ETA foils) is 3.5 x 10^{11} n cm^{-2}. This implies that the net neutron population with

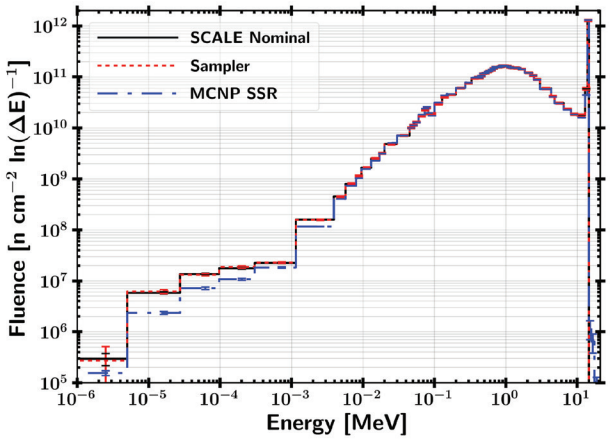

Figure 5. Comparison of MCNP SSR to SCALE 252-group unperturbed nuclear data and Sampler perturbed nuclear data at the ETA activation and HEU foils.

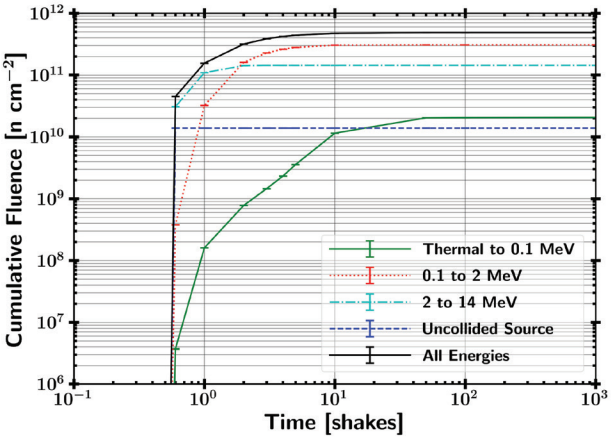

Figure 6. Cumulative neutron fluence on HEU foil as a function of time broken into four broad energy groups.

ETA is increased from the spherical divergence approximation, primarily due to reflection and (n,2n) reactions. The cumulative fluence on the HEU foil as a function of time is shown in Fig. 6.

The total neutron pulse length in the ETA cavity is approximately 10 shakes (100 nanoseconds). As expected based on the prompt nature of the NIF source, the total pulse length is much less than the half-lives of the activation products used in the unfolding, so the ingrowth and decay during the irradiation can be neglected. The uncollided source neutrons arrive at the foil in approximately 0.6 shakes, consistent with the time required for a 14.03-MeV neutron to travel from the source to the HEU foil.

JOURNAL OF RADIATION EFFECTS,
Research and Engineering
Vol. 38, No. 1, March 2020

The activation foil activities are summarized in Table 3. The mean value presented is the mean from the MCNP continuous energy results. The uncertainty presented is the statistical uncertainty of the MCNP continuous energy results combined in quadrature with the nuclear data uncertainty from the Sampler results. Uncertainty in the half-lives and branching ratios was small and could be neglected.

Table 3. Foil activities predicted with bootstrapped, nuclear data covariance uncertainty.

Product	$t_{1/2}$	Initial Activity [kBq]	$\Delta t = 2hr$ Activity [kBq]	Relative Error [%]
^{89}Zr	78.41 hrs	4.63	4.55	4.7
^{57}Ni	35.6 hrs	1.01	0.97	4.8
^{58}Co	70.86 days	0.74	0.74	2.5
^{196}Au	6.17 days	3.78	3.75	4.8
^{198}Au	2.69 days	2.98	2.92	2.6
$^{115}In^{m1}$	4.49 hrs	164	120	2.3
$^{116}In^{m1}$	54.29 min	1094	236	3.4
^{24}Na	15 hrs	13.8	12.6	4.6
^{187}W	24 hrs	5.79	5.46	4.1
^{56}Mn	2.58 hrs	23.5	13.7	20.0

Neutron Flux Unfolding Results

STAYSL was executed on all 182 sets of foil activities from Sampler to build a distribution of modeled experimental outcomes. The 129-group STAYSL unfolded results are shown in Fig. 7. The largest χ^2 trial and bootstrapped neutron fluence from all trials were added to Fig. 7 for comparison with the initial-guess MCNP spectrum with unperturbed nuclear data on the activation foil activities. The bootstrapped neutron fluence χ^2 represents the average value for the 182-trial samples. Additionally, the 5–95% activation ranges for each reaction are shown, indicating the region informed in the unfolding procedure by a given reaction.

The χ^2 results, derived from the unfolded activities, provide strong confidence in the ability to unfold the neutron spectrum from the foil activities with the degree of nuclear data covariance. The null hypothesis, that the two sets of data were governed from the expected distribution, could not be rejected for most of the trials with high confidence. The χ^2 for the nominal guess, largest sample, and bootstrapped unfolded activities are 0.36, 8.3, and 1.3 with p-values of 0.96, « 0.05, and 0.22, respectively. The p-values indicate the probability of achieving a larger χ^2 given the results, so the nominal case is within reasonable expectations, while the largest χ^2 value is rejected with strong significance. The bootstrapped activity p-value is closer to the rejection value of 0.05, but the p-value is large enough to not reject the unfolded activities. The distribution of χ^2/ν values for the set of trials is shown in Fig. 8.

Of the 182 trials, the hypothesis that activities come from the expected distribution was not rejected 81.9% of the time with 95% confidence. The distribution of χ^2 values peaks near 1; however, a non-negligible portion of the unfolding calculations provide results that rejected the null hypothesis.

It is nevertheless worth noting that even the rejected trials result in unfolded neutron energy spectra that are very similar, as shown for the largest sample χ^2 in Fig. 7. As described next, these small perturbations in the neutron

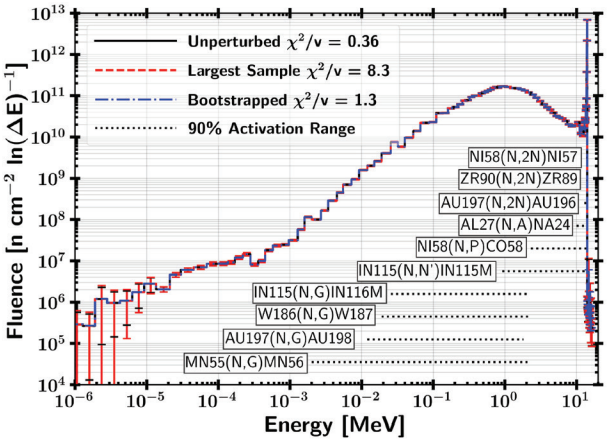

Figure 7. STAYSL unfolded spectra per unit lethargy for unperturbed nuclear data, largest deviation, and bootstrapped values.

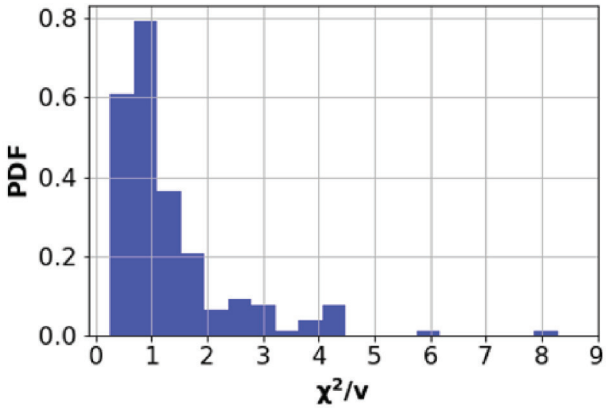

Figure 8. Probability density function of STAYSL unfolded ETA spectrum χ^2.

energy spectra result in negligible changes to the overall fission products produced in the HEU sample.

Fission Product Estimation Results

Table 4 displays the fission product production in the HEU foil using Nagy fits of experimental data. The uncertainties capture the uncertainties in the underlying energy-dependent fission product yield data, the uncertainties in the fit, the Monte Carlo statistical uncertainties, and the systematic nuclear data uncertainties from Sampler. The TN+PFNS objective-spectrum fission products are consistent with the fission product production achieved in the ETA within uncertainty associated with the modeled results. The Nagy and GEF models produce similar results, albeit with much higher uncertainty for the GEF results.

Table 4. ETA- and TN+PFNS-produced Nagy fit cumulative-fission product yield from experimental data.

Fission Product	Fission Product Yield [%]	
	ETA	TN+PFNS
^{91}Sr	5.34 ± 0.15	5.37 ± 0.08
^{92}Sr	5.38 ± 0.16	5.41 ± 0.10
^{95}Zr	6.03 ± 0.15	6.05 ± 0.06
^{97}Zr	5.71 ± 0.16	5.74 ± 0.08
^{99}Mo	5.62 ± 0.16	5.65 ± 0.08
^{103}Ru	3.20 ± 0.09	3.21 ± 0.05
^{105}Ru	1.41 ± 0.05	1.39 ± 0.04
^{109}Pd	0.32 ± 0.02	0.29 ± 0.02
^{111}Ag	0.28 ± 0.01	0.25 ± 0.01
^{112}Pd	0.27 ± 0.01	0.23 ± 0.01
^{113}Ag	0.20 ± 0.01	0.18 ± 0.01
^{115g}Cd	0.28 ± 0.01	0.25 ± 0.01
^{132}Te	4.32 ± 0.13	4.33 ± 0.07
^{140}Ba	5.56 ± 0.15	5.60 ± 0.07
^{141}Ce	5.46 ± 0.17	5.49 ± 0.10
^{143}Ce	5.06 ± 0.15	5.11 ± 0.09
^{144}Ce	4.69 ± 0.16	4.75 ± 0.11
^{147}Nd	2.08 ± 0.06	2.10 ± 0.03
^{149}Pm	1.01 ± 0.04	1.01 ± 0.03
^{151}Pm	0.47 ± 0.02	0.46 ± 0.02
^{153}Sm	0.18 ± 0.01	0.18 ± 0.01
^{156}Eu	0.028 ± 0.001	0.027 ± 0.001
^{161}Tb	0.0013 ± 0.00006	0.0011 ± 0.00004

The resultant GEF mass-chain distribution for the ETA and the original objective TN+PFNS are displayed in Fig. 9. Overall, there is large agreement in reproducing the fission product distribution expected from the TN+PFNS. The high uncertainty reflects the large parameter uncertainty in the GEF fission models that limit the ability to predict mass-chain fission products *a priori* across all mass chains.

The mass-chain, relative-residual yields comparing the ETA to the objective spectrum are shown in Fig 10. There are a few areas of disagreement between the mean value of the ETA and the TN+PFNS. The symmetric valley fission products are systematically larger because of the increased high-energy flux produced in ETA. Accordingly, there is a decrease in yield for asymmetric fission products' mass chains in ETA. However, the differences in the symmetric valley and asymmetric fission products are not substantial compared to the uncertainty in the fission product yield calculations.

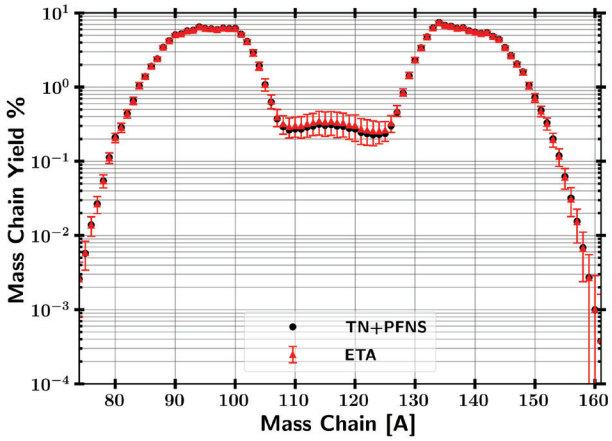

Figure 9. TN+PFNS versus ETA fission product mass-chain distributions calculated with GEF values.

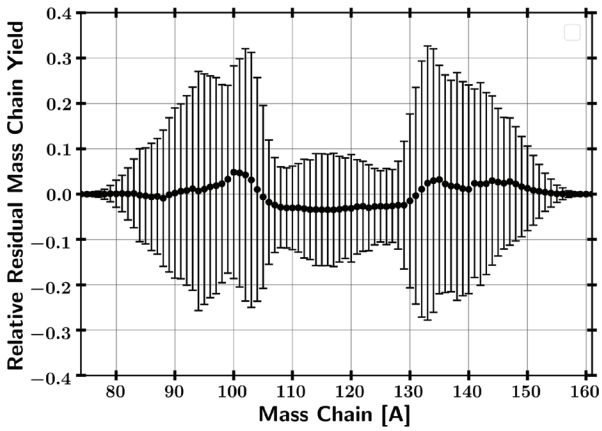

Figure 10. Relative-residual, mass-chain yields of ETA compared to TN+PFNS from GEF values.

JOURNAL OF RADIATION EFFECTS,
Research and Engineering
Vol. 38, No. 1, March 2020

Conclusion

This work describes the continued development, analysis, and support of the capability of producing spectrally accurate neutron environments through the use of an ETA. The application of this work focused on the production of fission fragment debris through targeted modification of the NIF source spectrum. The ETA design developed using Coeus replicates the neutron environment and fission product distributions of interest to technical nuclear forensics and provides a step forward in generating synthetic debris. The results model the full range of experimental outcomes and incorporate nuclear data covariance analysis to further bound the range of possible experimental outcomes for this novel approach to generating high-fidelity neutron environments. More analysis for this work and Coeus are available [8], [28].

The primary objective of the ETA research was to determine if the neutron energy distribution in a "typical" boosted nuclear weapon detonation can be produced using spectral modification with an ETA at the NIF. This research showed computationally that the ETA concept can fill the technical nuclear forensics and neutron environment capability gaps. The Pearson correlation coefficient and K-S two-sample statistic used to compare the TN+PFNS to the modeled-achieved neutron spectrum were 0.9 and 0.11, signifying that there is large spectral agreement in reproducing the objective neutron-fluence environment.

The ETA uses nontraditional nuclear materials and the measured results depend on independent channels in a weighting disproportional to the relative cross-sectional intensities. Therefore, SCALE Sampler was used to asses the impact of the nuclear data uncertainty on the measurable experimental outcomes. Using this approach, the nuclear data uncertainty and covariance on the ETA performance was found to be non-negligible. Nuclear data covariance increased the energy-dependent neutron fluence uncertainty in the ETA sample cavity to approximately 3–5% above 1 keV and 7–100% below 1 keV. The resultant nuclear data uncertainty, including the foil reaction cross-sectional uncertainty, resulted in uncertainties on the order of a few percent for all but the ^{55}Mn (n,γ) reaction where the systematic uncertainty was found to be 19.7%.

The foil activities and fission products produced in the ETA cavity are within measurable limits for radio-chemistry and gamma-ray spectroscopy. The measured fission products are used to unfold the neutron energy spectrum observed in the experimental cavity using STAYSL. The STAYSL unfolded results on each of the 182 Sampler trials provide an 80+% probability of being able to perform a statistically significant unfold of the neutron spectrum given a set of activation measurements and the modeled spectrum, based on the χ^2 of each unfolded trial.

In the context of technical nuclear forensics and attribution capabilities associated with device reconstruction, an observable quantity of interest is the fission product distribution created from the neutron flux interaction with the fissile material. The ETA's modeled performance produces 2 x 10^9 ±1% fissions, which is near the order of those collected in forensics ground samples. Selected fission products analyzed with the GEF code and experimental data from the literature were used to create energy-dependent Nagy fits. The fission products produced in the HEU with the ETA's spectral-shaping capability have an equivalent cumulative fission product yield distribution to the objective TN+PFNS within current fission product yield modeling capabilities.

The capability of producing objective neutron spectra has wide-reaching significance to further leverage operating neutron source facilities into new areas of research and support key capability needs. The ETA designed in this research effort contributes to further enable enhancements to nuclear attribution and has potential use for the certification of electronic components in neutron threat environments.

The future work related to the analysis performed here will compare the experimental outcomes to the predicted reactions and methodology used in this research. Although the ETA is a huge step forward for developing synthetic weapon debris, improvements will be made to develop a second-generation ETA to generate a more representative neutron spectrum. Additionally, facility improvements to the NIF and updated constraints will be incorporated to increase the optimization with the objective of increasing the efficiency of the ETA to produce 10^{11} fissions, which is essential to achieve better detection of low-yield fission products. Finally, real-world scenario nuclear fallout includes fractionation based on the physical properties and chemistry of the fission products. A fractionation technique can most readily focus on refractory fission products

with low-condensation points, as opposed to volatile mass chains, as many of these are gases that may be lost in chemical separations. Incorporating the fractionated, synthetic fission product debris into a matrix representative of a nuclear forensics collection would be of great benefit to technical nuclear forensics training and exercises.

References

[1] L. Zaidi, M. Belgaid, S. Taskaev, and R. Khelifi, "Beam shaping assembly design of ^{7}Li(p,n)^{7}Be neutron source for boron neutron capture therapy of deep-seated tumor," *Appl. Radiation and Isotopes*, vol. 139, pp. 316–324, May 2018.

[2] J.J. Molgaard, "Production of nuclear debris surrogates for forensic methods development," M.S. thesis, University of Tennessee-Knoxville, Knoxville, TN, p. 72, 2014.

[3] A.G. Osborne and M.R. Deinert, "Reducing irradiation damage in a long-life fast reactor with spectral softening," *Energies*, vol. 11, no. 6, p. 1507, June 2018.

[4] "National security and nuclear weapons in the 21st century," U.S. Dept. of Energy and U.S. Dept. of Defense, Tech. Rep., Sept. 2008.

[5] "Nuclear posture review," Office of the Secretary of Defense, Tech. Rep., 2018.

[6] *Nuclear Forensics: A Capability at Risk* (abbreviated version), Washington, DC: The National Academies Press, 2010.

[7] J. Bevins, "Targeted modification of neutron energy spectra for national security applications," Ph.D. dissertation, University of California-Berkeley, Berkeley, CA, 2017.

[8] J.E. Bevins, "Coeus V1.0," 2017. [Online]. Available: https://github.com/SlaybaughLab/Coeus/releases

[9] ——, "Gnowee V1.0," 2017. [Online]. Available: https://github.com/SlaybaughLab/Gnowee

[10] J.E. Bevins, S. Bogetic, L.A. Bernstein, R. Slaybaugh, and J. Vujic, "Metaheuristic optimization method for neutron spectra shaping," *Trans. Amer. Nucl. Soc.*, vol. 118, pp. 455–458, 2018.

[11] E. Bauge *et al.*, "Coherent investigation of nuclear data at Cea Dam: Theoretical models, experiments and evaluated data," *European Physical J. A*, vol. 48, no. 8, p. 113, 2012.

[12] N.J. Quartemont, A.A. Bickley, and J.E. Bevins, "Nuclear data covariance analysis in radiation transport simulations utilizing SCALE sampler and the IRDFF nuclear data library," *IEEE Trans. Nucl. Sci.*, 2020, [Online]. Available: https://ieeexplore.ieee.org/abstract/document/8977524

[13] M. Chadwick *et al.*, "ENDF/B-VII.1 nuclear data for science and technology: cross sections, covariances, fission product yields and decay data," *Nucl. Data Sheets*, vol. 112, no. 12, pp. 2887–2996, Dec. 2011.

[14] R. Capote, K. Zolotarev, V. Pronyaev, and A. Trkov, "International reactor dosimetry and fusion file IRDFF v.1.05," *J. ASTM Int.*, vol. 9, no. 4, Apr. 2012.

[15] J.R. Stickney, "Pulse height spectra analysis of a neutron energy tuning assembly," Ph.D. dissertation, AFIT, Wright-Patterson AFB, OH, 2018.

[16] T. Goorley *et al.*, "Initial MCNP6 release overview," *Nucl. Technol.*, vol. 180, no. 3, pp. 298–315, 2012.

[17] S. Nagy, K.F. Flynn, J.E. Gindler, J.W. Meadows, and L.E. Glendenin, "Mass distributions in monoenergetic-neutron-induced fission of ^{238}U," *Physical Rev. C*, vol. 17, no. 1, pp. 163–171, 1978.

[18] L. Glendenin, J. Gindler, D. Henderson, and J.W. Meadows, "Mass distributions for monoenergetic-neutron-induced fission of ^{235}U," *Physical Rev. C*, vol. 24, no. 6, pp. 2600–2605, 1981.

[19] G.P. Ford and R.B. Leachman, "Fission mass yield dependence on angular momentum," *Physical Rev.*, vol. 137, no. 4 B, 1965.

[20] M.E. Gooden *et al.*, "Energy dependence of fission product yields from ^{235}U, ^{238}U and ^{239}Pu for incident neutron energies between 0.5 and 14.8 MeV," *Nucl. Data Sheets*, vol. 131, pp. 319–356, 2016.

[21] M.E. Gooden, "Energy dependence of fission product yields from ^{235}U, ^{238}U, and ^{239}Pu for incident neutron energies between 0.5 and 14.8 MeV," Ph.D. dissertation, NC State, Raleigh, NC, 2014.

[22] D.R. Nethaway and G. Barton, "A compilation of fission product yields in use at the Lawrence Livermore Laboratory," Tech. Rep., 1973.

[23] T.C. Chapman, G.A. Anzelon, G.C. Spitale, and D.R. Nethaway, "Fission product yields from 6–9 MeV

neutron-induced fission of ^{235}U and ^{238}U," *Physical Rev. C*, vol. 17, no. 3, pp. 1089–1097, Mar. 1978.

[24] T.R. England and B.F. Rider, "Evaluation and compilation of fission product yields," LANL, Los Alamos, NM, Tech. Rep. LA-UR-94-3106, pp. 1–173, 1994.

[25] J.G. Cuninghame, J.A.B. Goodall, and H.H. Harris, "Absolute yields in the fission of ^{235}U by monoenergetic neutrons of energy 130–1700 keV," *J. Inorganic Nucl. Chemistry*, vol. 36, no. 7, pp. 1453–1457, 1974.

[26] C.B. Yeamans and B.E. Blue, "National Ignition Facility neutron sources," LLNL, Livermore, CA, Tech. Rep. LLNL-CONF-739397, 2018.

[27] K.B. Fournier, "NIF and OMEGA x-ray environments summary," LLNL, Livermore, CA, Tech. Rep. LLNL-TR-666017, 2015.

[28] N.J. Quartemont, "NIF-ETA," 2019. [Online]. Available: https://github.com/nickquartemont/NIF ETA

[29] G.F. Knoll, *Radiation Detection and Measurement*, 4th ed., Ann Arbor, MI: Wiley, 2010.

[30] E. Vagena, K. Theodorou, and S. Stoulos, "Thick-foils activation technique for neutron spectrum unfolding with the MINUIT routine—comparison with GEANT4 simulations," *Nucl. Instruments and Methods in Physics Res., Section A: Accelerators, Spectrometers, Detectors and Associated Equipment*, vol. 887, no. 11, pp. 64–69, Apr. 2018.

[31] X-5 Monte Carlo Team, "MCNP—A general Monte Carlo N-Particle transport code, version 5," LANL, Los Alamos, NM, Tech. Rep. LA-UR-03-1987, 2008.

[32] B. Rearden and M. Jessee, eds., *SCALE Code System*, ORNL/TM-2005/39, Version 6.2.3, Oak Ridge National Laboratory, Oak Ridge, TN, Mar. 2018. Available: Radiation Safety Information Computational Center, CCC-834.

[33] L. Greenwood and C. Johnson, "Least-squares neutron spectral adjustment with STAYSL PNNL," *EPJ Web of Conf.*, vol. 106, p. 07001, 2016.

[34] B. Appelbe and J. Chittenden, "Relativistically correct DD and DT neutron spectra," *High Energy Density Physics*, vol. 11, no. 1, pp. 30–35, 2014.

[35] R. Khan, S. Karimzadeh, T. Stummer, and H. Böck, "Monte Carlo simulation of the thermal column and beam tube of the TRIGA Mark II research reactor," *Nucl. Eng. Design*, vol. 241, no. 8, pp. 2859–2864, 2011.

[36] T. Siegl and A. West, "Statistical bootstrapping methods in VaR calculation," *Appl. Math. Finance*, vol. 8, no. 3, pp. 167–181, 2002.

[37] B. Rearden and M. Jessee eds., *User Guide for the STAYSL PNNL Suite of Software Tools, PNNL-22253*, Pacific Northwest National Laboratory, Richland, WA, Feb. 2013.

[38] F.G. Perey, *Least-Squares Dosimetry Unfolding: The Program STAY'SL (ORNL/TM-6062)*, Oak Ridge, TN, 1977.

[39] J.R. Taylor, *An Introduction to Error Analysis: The Study of Uncertainties in Physical Measurements*, 2nd ed., South Orange, NJ: University Science Books, 1997.

[40] K.-H. Schmidt, B. Jurado, C. Amouroux, and C. Schmitt, "General description of observables in low-energy fission: GEF model code," *Nucl. Data Sheets*, vol. 131, pp. 107–221, Jan. 2016.

[41] K.-H. Schmidt and B. Jurado, "General description of fission observables," JEFF Rep. 24, 2014.

[42] M.J. Wang, R.J. Sheu, J.J. Peir, and J.H. Liang, "Criticality calculations of the HTR-10 pebble-bed reactor with SCALE6/CSAS6 and MCNP5," *Annals Nucl. Energy*, vol. 64, pp. 1–7, 2014.

[43] S.R. Johnson and K.T. Clarno, "Comparison of SCALE and MCNP results for computational pebble bed benchmarks," *Trans. Amer. Nucl. Soc.*, vol. 96, pp. 420–422, Jan. 2007.

[44] Y.F. Chen, R.J. Sheu, S.H. Jiang, J.N. Wang, and U.T. Lin, "Surface dose rate calculations of a spent-fuel storage cask by using MAVRIC and its comparison with SAS4 and MCNP," *Nucl. Technol.*, vol. 175, no. 1, pp. 343–350, 2011.